



Sol–Gel SiO₂ on electrospun polyacrylonitrile nanofiber for efficient oil-in-water emulsion separation

Zong-Yao Ying^{1,2,3}, Zai-Dong Shao², Lin Wang², Xuan Cheng^{1,3,*}, and Yu-Ming Zheng^{2,*}

¹Department of Materials Science and Engineering, College of Materials, Xiamen University, Xiamen 361005, China

²CAS Key Laboratory of Urban Pollutant Conversion, Institute of Urban Environment, Chinese Academy of Sciences, 1799 Jimei Road, Xiamen 361021, China

³Fujian Key Laboratory of Advanced Materials, Xiamen University, Xiamen 361005, Fujian, China

Received: 27 April 2020

Accepted: 21 August 2020

Published online:
4 September 2020

© Springer Science+Business
Media, LLC, part of Springer
Nature 2020

ABSTRACT

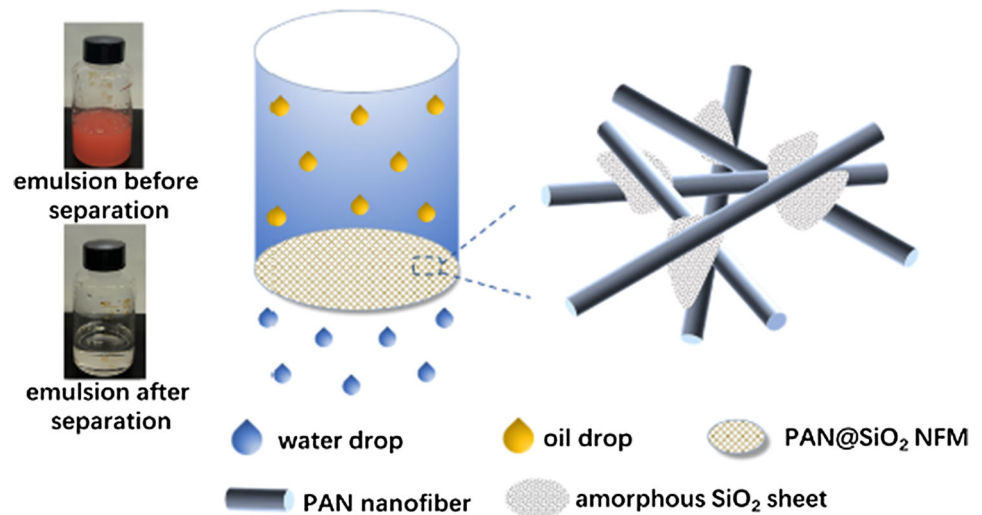
A membrane for efficient oil-in-water emulsion separation requires a surface with hydrophilic/underwater oleophobic properties. In this study, a simple and facile sol–gel strategy was proposed for preparing oil-in-water emulsion separation membrane with hydrophilic/underwater oleophobic surface by growing amorphous SiO₂ sheets on an electrospun polyacrylonitrile nanofiber membrane (PAN NFM). The composite membranes (PAN@SiO₂ NFMs) showed excellent properties in mechanical strength, hierarchical microporous structure, hydrophilicity and underwater oleophobicity, as well as remarkable performance in water flux, separation efficiency and cyclic stability. Under a low pressure of 1 kPa driven by the self-weight of emulsion, the PAN@SiO₂ NFM demonstrated a large flux of $3994.3 \pm 356.0 \text{ L m}^{-2} \text{ h}^{-1}$ and a high separation efficiency of 99.50%. In ten successive cycle tests, fluxes of the PAN@SiO₂ NFM remained above $3000 \text{ L m}^{-2} \text{ h}^{-1}$, while the residual TOC in filtrate was stable at around 30 mg L^{-1} , indicating the PAN@SiO₂ NFM has excellent cyclic stability. It is also demonstrated that the PAN@SiO₂ NFM is suitable for the separation of various kinds of emulsions, such as toluene, *n*-heptane, paraffin liquid, *n*-hexane and xylene. Hence, the prepared PAN@SiO₂ NFM is a promising hydrophilic/underwater oleophobic membrane for efficient emulsion separation.

Handling Editor: Chris Cornelius.

Zong-Yao Ying and Zai-Dong Shao have contributed equally to this work and should be considered as co-first authors.

Address correspondence to E-mail: xcheng@xmu.edu.cn; ymzheng@iue.ac.cn

GRAPHIC ABSTRACT



Introduction

Rapid population and economic growth have increased the demand for clean water [1], which has exceeded the resource of the earth [2]. Moreover, hazardous oil pollution as a result of the discharge of oily effluents aggravated the water scarcity [3, 4]. Therefore, the problem of oily wastewater pollution must be solved. According to the diameter of oil droplets in water, oil pollution in water can be divided into three types, namely free ($> 150 \mu\text{m}$), dispersed ($20\text{--}150 \mu\text{m}$) and emulsified oil pollution ($< 20 \mu\text{m}$). Given the large droplet size of free and dispersed oils, they are immiscible with water and can be easily removed, whereas emulsified oil is difficult to clean up because it disperses well in water [5]. Therefore, the separation of oil/water emulsion is the key for oily wastewater treatment.

Conventional emulsion separation methods include chemical demulsification, air flotation, adsorption, biotreatment and so on [6–9]. These traditional separation methods may have disadvantages, such as complex operation process, low separation efficiency and high operating cost, so it is necessary to develop simple and effective approach for emulsion separation [10]. Studies on membrane

technology for emulsion separation have been increasing. As a selective permeation material, membrane can be acted as a filter to intercept target pollutants and achieve the purpose of pollutant separation and purification when contaminated water flows through the membrane. According to the pore size, membrane separation methods can be divided into microfiltration, ultrafiltration, nanofiltration and reverse osmosis [11–14]. Compared with other conventional treatment methods, membrane separation shows high separation efficiency, low cost and controllable process [15]. This method is promising for separating emulsions, although it has several limitations, such as low flux and membrane fouling tendency due to the blockage of oil droplets [16, 17]. Therefore, the preparation of a membrane with a high separation efficiency, large flux, stable cyclic performance and low cost should be studied further.

Nanofiber membrane is a novel membrane separation material, of which the separation efficiency increases with decreasing fiber diameter [18] because of the large Brunauer–Emmett–Teller (BET) specific surface area, high porosity and superior fiber uniformity [19]. Methods for nanofiber preparation, including tensile [20], template synthesis [21] and self-assembly [22], are widely used, but may have

limitations in terms of equipment requirements, process controllability, spinnability range, cost, productivity or fiber size controllability [23–27]. Thus, these methods should be further optimized for preparing highly efficient membrane separation materials. As a method for preparing nanofibers, electrospinning has outstanding advantages of continuous mass production of nanofibers, mild preparation conditions, wide application range [28], simple operation process and high production rate [29]. Therefore, electrospinning could be a good choice for preparing nanofiber membranes as emulsion separation material [30].

Several important issues limit the application of electrospun membranes for emulsion separation. For example, membrane fouling is an issue of concern, which could lead to a gradual deterioration of membrane performance [31, 32]. Efficient oil-in-water emulsion separation usually requires a hydrophilic/underwater oleophobic membrane, which can be achieved by creating a high roughness surface and high-surface-energy materials. The improvement of membrane hydrophilicity can reduce the oil fouling and enhance the water flux [33]. Thus, in the present study, we composite a hydrophilic electrospun nanofiber membrane. SiO₂ is one of the most common materials used for hydrophilicity modification [34, 35], with low cost, good thermal and mechanical stability and mild reactivity [36]. Hence, SiO₂ is frequently used to composite NFMs to reduce membrane fouling and increase water flux. *Shan* et al. [37] used aldehyde benzoxazine as an in situ polymerization monomer to introduce SiO₂ nanoparticles onto pristine nanofibers. The gravity-driven water flux reached 2237 L m⁻² h⁻¹, and the separation performance was stable in ten cycles. *Ge* et al. [16] combined electrospinning with electrostatic spray to obtain SiO₂ particles on the fiber surface to enhance the surface roughness and increase the hydrophilicity. The fluxes of surfactant-free and surfactant-stabilized petroleum ether emulsions reached 6456 and 926 L m⁻² h⁻¹, respectively. *Tai* et al. [38] chose TEOS as the silicon source and PAN as the carbon source to fabricate a PAN-SiO₂ NFM by electrospinning. The PAN-SiO₂ NFM was further carbonized at 900 °C to obtain a SiO₂-carbon composite NFM as an emulsion separation material. The NFM is resistant to increased temperature (up to 350 °C) and stable toward a wide range of pH (2–14). Although there have been many reports on the fabrication of

composite electrospun nanofiber membranes for emulsion separation, their practical applications were limited by the complicated preparation process and high energy consumption.

The aim of this study is to simplify the preparation of composite membrane while maintaining excellent separation performance. A facile sol-gel strategy was developed to compound amorphous SiO₂ sheets on the surface of electrospun NFM. Given its intrinsic hydrophilicity and stability [39, 40], polyacrylonitrile (PAN) was used as a substrate to fabricate the pristine NFM. Tetraethyl orthosilicate (TEOS) was selected as the hydrophilic silicon source, and hydrophilic SiO₂ was derived from hydrolysis and polycondensation of TEOS. A large piece of the composite membrane can be manufactured under a moderate condition. The results demonstrated that PAN@SiO₂ NFM has excellent oil/water separation performance, and it may be a promising material for the separation of various emulsions.

Experimental section

Materials

PAN (M_w = 90,000) was commercially purchased from Kunshan Hong Yu Plastic Co., Ltd (Suzhou, China). TEOS (AR, ≥ 28.4%), N,N-dimethylformamide (DMF, AR, ≥ 99%), ethanol absolute (EtOH, AR, ≥ 99.7%), ammonium hydroxide (NH₄OH, GR, 25%–28%), hydrochloric acid (HCl, AR, 36%–38%), toluene (AR, ≥ 99.5%), *n*-hexane (AR, ≥ 97%), xylene (AR, ≥ 99.0%) and Tween 80 (65.0–80.0 mg-KOH/g) were purchased from Sinopharm Chemical Reagent Co., Ltd (Shanghai, China). *n*-heptane (AR, ≥ 97%) and paraffin liquid (CP, T_{distillate} ≥ 300 °C) were obtained from Tianjin Guangfu Fine Chemical Research Institute (Tianjin, China).

Preparation of PAN nanofiber membrane

The PAN NFM was fabricated via electrospinning. First, PAN powder was added to DMF and then mixed with a stirring speed of 300 r min⁻¹ for 6 h at room temperature to obtain a 10 wt% PAN solution. The PAN solution was loaded into an injection syringe and fed by an injection pump (LSP01-1A, Longer Pump, China) with an injection rate of 1 mL h⁻¹ for 1 h. Under the action of an electric field, PAN

nanofibers were received by a sheet of nonwoven fabric on the collector for support. The voltage between the nozzle and the collector was 18 kV, and the distance was 15 cm. The temperature was kept at 25 ± 2 °C, and the humidity was maintained at $45 \pm 3\%$ by using a dehumidifier (DH-8138C, KAWASIMA, China). After electrospinning, the PAN NFM was plasticized with a plastic machine (G236R-013, Deli, China) to increase the bonding energy between the nonwoven fabric and PAN NFM.

Preparation of TEOS-based silica sol

In a typical preparation process, 5.5 mL of TEOS was dissolved in 2.7 mL of DI water and 14 mL of ethanol. To promote the TEOS hydrolysis, 0.2 mL of diluted acid (HCl:ethanol = 1:49) was mixed with the solution. Subsequently, the solution was mixed with a stirring rate of 300 r min^{-1} for 12 h at room temperature to ensure complete hydrolysis of TEOS. After hydrolysis for 12 h, the silica sol was diluted by ethanol to obtain solutions with dilution factors of 10, 15, 20 and 30 times. Finally, 0.5 mL of NH_4OH was added to each dilute TEOS-based silica sol solution and stirred with a speed of 300 r min^{-1} for 0.5 h to promote TEOS polycondensation.

Preparation of PAN@SiO₂ nanofiber membrane

A facile sol–gel strategy was developed to fabricate the PAN@SiO₂ NFM, and the preparation process is shown in Fig. 1. During the sol–gel process of TEOS, the PAN NFM was immersed in the diluted TEOS sol on a piece of glass. A glass rod was used to ensure

that the sol infiltrated the PAN NFM uniformly and to remove the residual sol. The TEOS sol would polycondense between the fibers of the PAN NFM. In the end, the membrane was dried at 60 °C for 2 h to form a composite membrane. Different dilution factors of TEOS sol were marked as P@S-1, P@S-2, P@S-3 and P@S-4 corresponding to 10, 15, 20 and 30 times, respectively.

Preparation of oil-in-water emulsions

Several kinds of oil-in-water emulsions without surfactant (SFEs) and with surfactant (SSEs) were prepared to evaluate the separation performance of PAN and PAN@SiO₂ NFMs. Oil/water mixtures were prepared by adding oils (toluene, *n*-heptane, paraffin liquid, *n*-hexane and xylene) to the water in a ratio of 1:100 (v/v). SFEs were obtained by sonicating the oil/water mixtures under a power of 500 W for 2 h. SSEs were prepared by adding surfactant Tween 80 to the oil/water mixtures and then sonicated under a power of 500 W for 2 h to obtain a milky white solution. The content of Tween 80 was 0.1 mg mL^{-1} .

Characterization

The PAN NFM was fabricated using an electrospinning machine (NEU-01, TongLi, China). Scanning electron microscope (SEM) images and energy-dispersive X-ray spectroscopy (EDX) spectra were obtained from a field emission SEM (S-4800, Hitachi, Japan). The surface roughness was measured with an atomic force microscope (AFM, MultiMode 8, BRUKER Nano Surfaces Business). Fourier transform infrared (FT-IR) spectra were derived from a Fourier

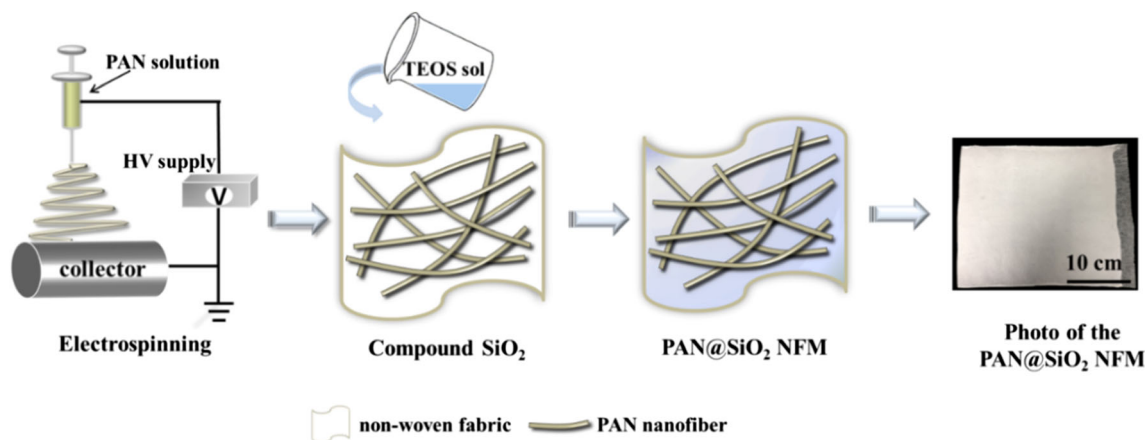


Figure 1 Schematic diagram of the preparation of PAN@SiO₂ NFM.

transform infrared spectrometer (iS10, Thermo Electron Corporation). Thermogravimetric analysis (TGA) was tested with a thermal gravimetric analyzer (TG 209 F3, Netzsch, Germany). Water contact angle (WCA) and underwater oil contact angle (UOCA) were measured with a video optical contact angle measuring device (DSA20, KRUSS, Germany). Nitrogen adsorption–desorption isotherms were measured by a high-precision gas/vapor adsorption measurement instrument (BELSORP-max, MicrotracBEL, Japan). BET specific surface area was obtained by BET model, and mesopore and micropore diameter distribution curves were obtained by Barrett–Joyner–Halenda (BJH) and Horvath–Kawazoe (HK) models, respectively. The optical microscope images of the toluene emulsions were taken using a laser confocal Raman spectrometer (LabRAM Aramis, Horiba, Japan). Tensile stress properties were measured with a universal testing machine (KD-II 100 N, KaiQiangLi, China), and the stretching velocity was controlled at 1 mm min⁻¹. Membrane pore diameter distribution was analyzed using a capillary flow porometer (POROMETER 3Gzh, Quantachrome). Emulsion particle size was measured through a zeta potential and nano-/submicron particle size analyzer (ZetaPALS, Malvern, England).

Oil-in-water emulsion separation performance test

The oil-in-water emulsion separation performance of PAN and PAN@SiO₂ NFMs was characterized using emulsion separation efficiency and membrane flux.

Emulsion separation efficiency (R) was calculated by the following equation:

$$R = \frac{V_e - V_r}{V_e} \times 100\%$$

where V_e presents the total organic carbon (TOC) concentration of the emulsion and V_r is the residual TOC concentration of the emulsion after separation.

TOC concentration was measured using a TOC analyzer (dry method, TOC-Vcph, Shimadzu, Japan). Membrane flux was calculated by the change rate of water flow, and the tested area of the NFM was 10.2 cm². Extremely thin nonwoven fabric with a thickness of 210 μm and average pore size of 647 μm was selected as the supporting material. In evaluating the cycle performance and stability of the membrane for

emulsion separation, the tested NFM was rinsed with ethanol before the next cycle test.

Results and discussion

Surface morphology and chemical composition of the PAN@SiO₂ NFM

The surface and cross-sectional morphology of a typical PAN NFM and PAN@SiO₂ NFM (P@S-3) was observed by SEM. PAN nanofibers showed a uniform distribution of irregular orientation (Fig. 2a₁). The statistical diameter distribution of the PAN nanofibers obtained from SEM image is shown in Fig. 2a₂. The diameter distribution conformed to the Gaussian distribution, that is, concentrated within 300–400 nm, indicating the good uniformity of the PAN nanofibers' diameter. The preparation of PAN@SiO₂ NFM was through the condensation of TEOS sol between the PAN nanofibers to form a composite structure of amorphous SiO₂ sheets and PAN nanofibers. After compounding, amorphous SiO₂ sheets were distributed evenly between fibers (Fig. 2b₁ and b₂). Amorphous SiO₂ sheets were made up of granular SiO₂ due to the condensation of TEOS sol. The content of amorphous SiO₂ sheets tapered off from P@S-1 to P@S-4 as predicted given the different dilution factors of TEOS sol (Figs. 2b₁, S1, S2 and S3). The pores of the PAN@SiO₂ NFM were formed by the staggered distribution of the PAN nanofibers and the interspaces between the SiO₂ sheets (Figs. 2b₁, b₂). Compared with PAN NFM, the pore diameter of PAN@SiO₂ NFM decreased significantly due to the loading of amorphous SiO₂ sheets, which laid a foundation for improving the emulsion separation efficiency. As illustrated in Fig. S4, influence of drying temperature on morphology of the amorphous SiO₂ sheets were analyzed by SEM image observation. The results demonstrated that drying temperature had insignificant effect on the morphology of the amorphous SiO₂ sheets. According to the cross-sectional images (Fig. 2c₁ and c₂), the thickness of the as-prepared PAN@SiO₂ NFM was only about 15 μm. Amorphous SiO₂ sheets were evenly distributed among the fibers.

To better understand the detailed information of SiO₂ sheets, the PAN@SiO₂ NFM was immersed in DMF to obtain the amorphous SiO₂ sheets. The thickness and surface roughness of the SiO₂ sheets

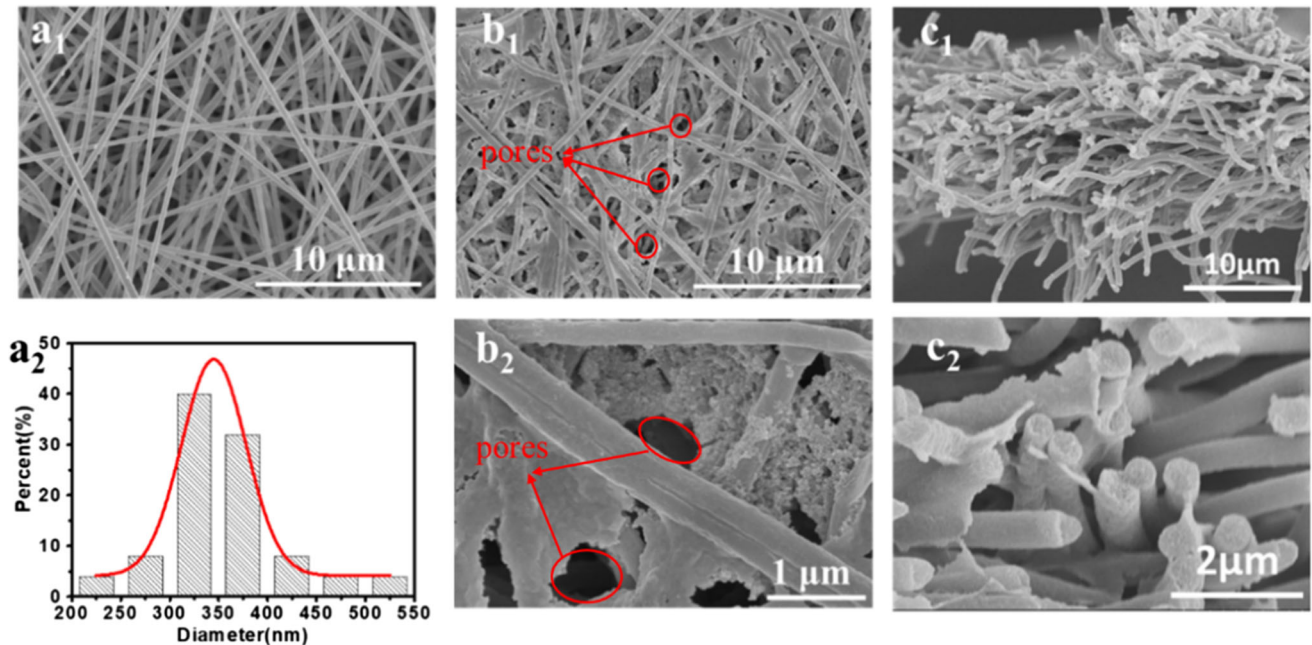


Figure 2 **a**₁ SEM image, **a**₂ fiber diameter distribution of the PAN NFM, **b**₁, **b**₂ surface and **c**₁, **c**₂ cross-sectional SEM images of the PAN@SiO₂ NFM.

were analyzed by cross-sectional SEM and AFM observation. As shown in Fig. S5, the thickness of three typical SiO₂ sheets was 57.5, 67.0 and 67.4 nm, respectively, and the average thickness was 64.0 nm, showing the uniformity of the SiO₂ sheets thickness. The formation of wrinkles on the AFM image of the SiO₂ sheet could be due to the dissolution of PAN nanofibers, and the average surface roughness (*R*_a) was determined to be 5.84 nm (Fig. S6).

The FT-IR spectra are shown in Fig. 3a. The pure PAN NFM exhibited a characteristic absorption peak at 2244 cm⁻¹, which is assigned to the stretching vibration of C≡N groups, and the absorption peak at 2921 cm⁻¹, which is the stretching vibration of C–H groups. The bending vibration peak of CH₂ groups appears at 1453 cm⁻¹. Compared with the PAN NFM, all the PAN@SiO₂ NFMs showed similar characteristic bands of SiO₂. The absorption peaks at 1080 and 800 cm⁻¹ correspond to the antisymmetric stretching vibration peak and symmetric stretching vibration peak of the Si–O–Si groups, respectively. The absorption peak at 960 cm⁻¹ is the swing vibration absorption peak of the Si–OH groups. The EDX spectra of PAN and PAN@SiO₂ NFMs are shown in Fig. S7. Given that the constituent elements of PAN are H, C and N, the EDX analyses of PAN NFM detected distinct Kα1 peaks for C and N. PAN@SiO₂

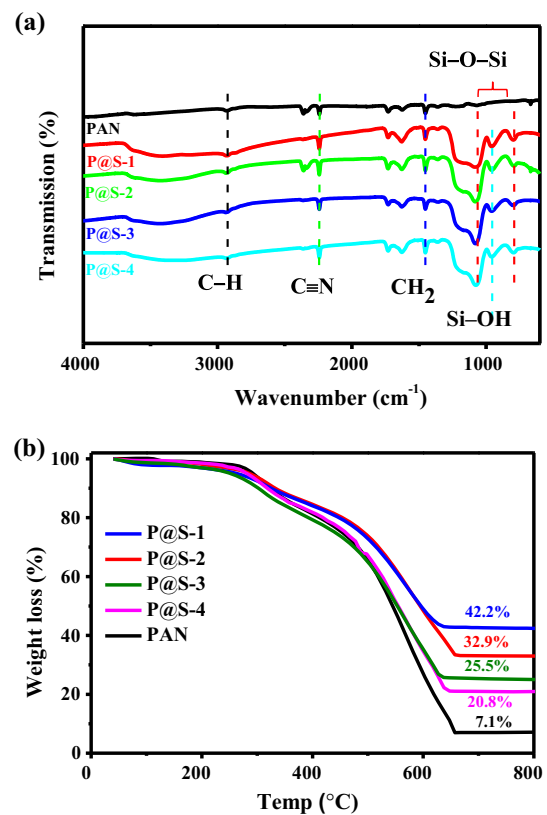


Figure 3 **a** FT-IR spectra, **b** TGA curves of PAN and PAN@SiO₂ NFMs.

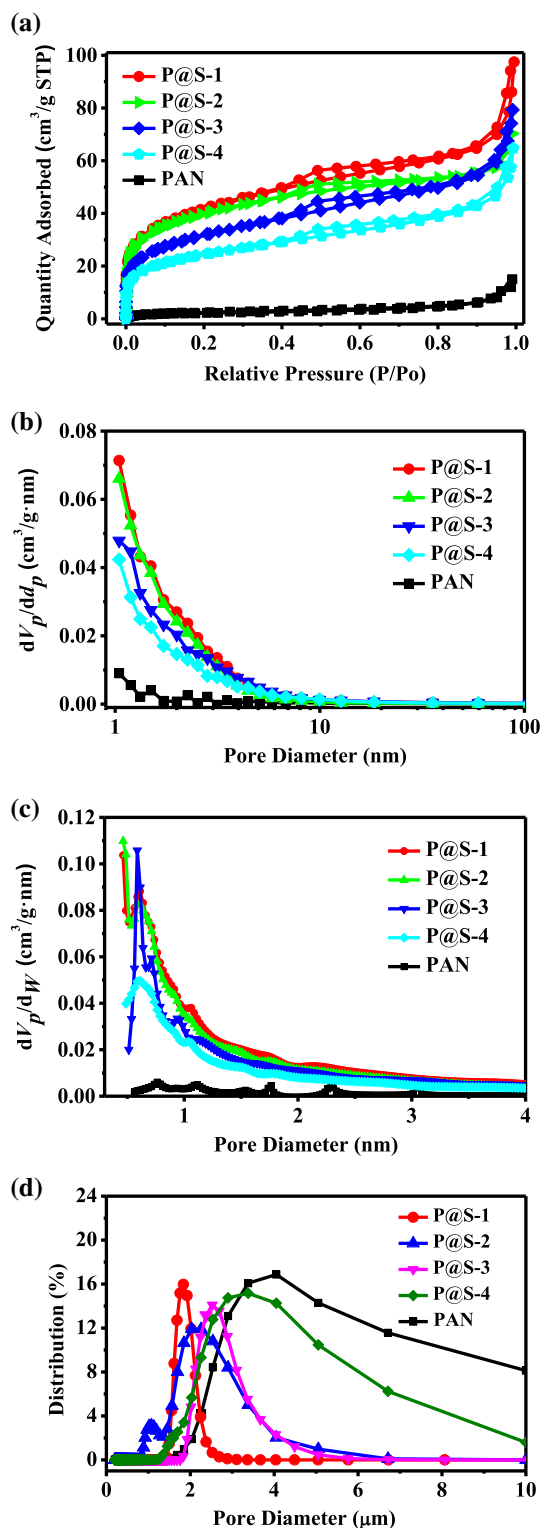
Figure 4 **a** Nitrogen adsorption–desorption isotherms of PAN and PAN@SiO₂ NFMs, **b** mesopore size distribution of PAN and PAN@SiO₂ NFMs obtained by BJH model, **c** micropore size distribution of PAN and PAN@SiO₂ NFMs obtained by HK model, **d** macropore size distribution of PAN and PAN@SiO₂ NFMs.

NFM also had peaks of Si and O, indicating the possibility of the existence of SiO₂. Combined with the results of FI-IR spectra, SiO₂ was successfully composited onto the surface of the PAN NFM.

Thermal stability and SiO₂ composition of the PAN@SiO₂ NFMs were analyzed by TGA (Fig. 3b). For the pure PAN NFM, the desorption of a small amount of adsorbed water was observed below 280 °C. When the temperature was higher than 280 °C, an evident weight loss occurred due to the oxidation decomposition of PAN NFM, and the gradual weight loss continued till 650 °C, leaving only 7.1% of the weight. The weightlessness trend of the four PAN@SiO₂ NFMs was similar to that of PAN NFM, which decreased from room temperature to approximately 650 °C. After calcination, white SiO₂ powder was obtained, and the residual weights of P@S-1, P@S-2, P@S-3 and P@S-4 were 42.2%, 32.9%, 25.5% and 20.8%, respectively. The apparent weightlessness was due to the oxidation decomposition of the PAN NFM. Thus, the SiO₂ content of PAN@SiO₂ NFMs was 35.1, 25.9, 18.4 and 13.7 wt%, respectively, corresponding to P@S-1, P@S-2, P@S-3 and P@S-4. The SiO₂ content was closely related to the physical properties and oil-in-water emulsion separation performance of the PAN@SiO₂ NFMs.

Mechanical and porous properties of the PAN@SiO₂ NFM

Mechanical properties are important to the practical application of NFMs. Tensile stress–strain curves of the PAN and PAN@SiO₂ NFMs are shown in Fig. S8. Compared with the PAN NFM, the tensile modulus of PAN@SiO₂ NFMs was significantly improved. It was found that the tensile modulus of PAN@SiO₂ NFMs raised with the increase in SiO₂ content, but the fracture strain decreased. The values are listed in Table S1. As shown in Fig. 2b, amorphous SiO₂ sheets interconnected the PAN nanofibers, leading to the mechanical strength enhancement of the PAN@SiO₂



NFMs. Hence, the composite of SiO₂ could enhance the mechanical strength of the PAN@SiO₂ NFMs.

The porous structure of NFMs tested by nitrogen adsorption–desorption and capillary flow is shown in Fig. 4; it was found that the PAN@SiO₂ NFMs exhibited a hierarchical porous structure. Figure 4a shows the nitrogen adsorption–desorption isotherms of the PAN and PAN@SiO₂ NFMs at 77 K. According to Fig. 4a, the PAN NFM demonstrated a macroporous structure. However, the PAN@SiO₂ NFMs exhibited type IV isotherms and type H2 hysteric loops, which are typical mesoporous structures. The pore structure of PAN@SiO₂ NFMs is a mixed type of slit and ink bottle. The abundant porous structure can improve the separation performance of PAN@SiO₂ NFMs. As can be seen from the mesopore diameter distribution curves of PAN@SiO₂ NFMs in Fig. 4b, the pore size is mainly less than 10 nm. Further, it was found that the pore size was concentrated below 1 nm according to the micropore diameter distribution curves of PAN@SiO₂ NFMs as shown in Fig. 4c. Compared with the PAN NFM, the pore size of PAN@SiO₂ NFMs decreased significantly. BET specific surface area and BJH pore volume of PAN@SiO₂ NFMs are much higher than that of the PAN NFM, which was positively correlated with the SiO₂ content; the specific values are listed in Table 1. The abundant microporous and mesoporous channels of PAN@SiO₂ NFMs could significantly facilitate the liquid transport driven by the capillary force, which would be beneficial for enhancing the oil/water separation performance.

The size of the emulsion droplets that can be intercepted depends on the macropore size of the membrane. Thus, the measurement of macropore size distribution of PAN and PAN@SiO₂ NFMs is essential to study the interception behavior of emulsion droplets during the separation process. The macropore size distribution of PAN and PAN@SiO₂ NFMs are shown in Fig. 4d. It can be seen that the average macropore size of NFMs decreased with the increment of SiO₂ content. The average macropore size of PAN, P@S-1, P@S-2, P@S-3 and P@S-4 is 3.38, 1.68,

1.89, 2.52 and 2.89 μm, respectively. The results demonstrated that the amorphous SiO₂ sheets play a crucial role in reducing the macropore size, which could improve the oil-in-water emulsion separation efficiency. The novel hierarchical porous structure of PAN@SiO₂ NFMs could be benefit to improve the oil-in-water emulsion separation performance.

Wetting behavior of the PAN@SiO₂ NFM

A hydrophilic and underwater oleophobic surface is required in oil-in-water emulsion separation. In the separation process, a hydrophilic surface can not only relieve membrane fouling caused by oil but also increase the water flux. Water contact angles were measured to evaluate the wetting behavior of PAN and PAN@SiO₂ NFMs.

To analyze the wetting behavior of the PAN and PAN@SiO₂ NFMs, the process of water droplet infiltrating the NFMs surface was recorded by video (Video S1 and S2). The hydrophilicity of PAN and PAN@SiO₂ NFMs was characterized by the change of WCA over time (Fig. 5a). When 4 μL of water was dropped on the PAN NFM surface, the WCA decreased from 130° to 40° in 5 s due to the intrinsic hydrophilicity of the PAN and then stabilized at a relatively stable state. As a comparison, the WCA of the PAN@SiO₂ NFMs fell rapidly to approximately 10° from WCA of less than 60°, thereby showing better hydrophilicity than the pure PAN NFM. Given the hydrophilicity of SiO₂, the infiltration time decreased with the increase in SiO₂ content. Water is more likely infiltrated into the PAN@SiO₂ NFMs, resulting in increased water flux.

A superior oil-in-water emulsion separation membrane requires that water can be easily infiltrated in; however, the oil should be effectively rejected. Thus, the underwater oleophobicity is another important factor, which significantly affects the separation efficiency of oil-in-water emulsion. To analyze the underwater oleophobicity of the NFMs, Sudan III-colored CCl₄ was selected as the tested oil. The results illustrated that the UOCA increased

Table 1 Specific surface area, pore volume and average pore diameter of the PAN and PAN@SiO₂ NFMs

	PAN	P@S-1	P@S-2	P@S-3	P@S-4
S_{BET} (m ² g ⁻¹)	8.62	144.32	137.07	110.29	84.89
V_{BJH} (cm ³ g ⁻¹)	0.023	0.152	0.109	0.123	0.101
Average pore diameter (nm)	10.85	4.20	3.19	4.47	4.74

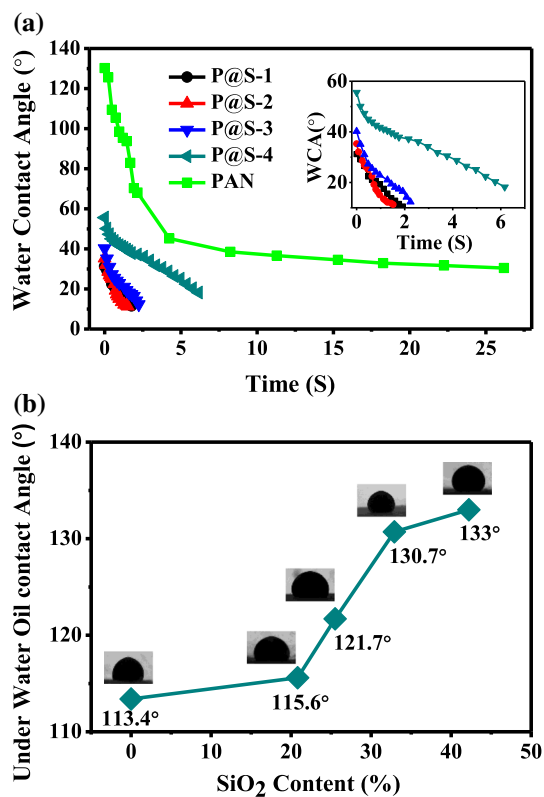


Figure 5 a Wettability of PAN and PAN@SiO₂ NFMs, insert picture was the zoom in figure in 0–7 s of PAN@SiO₂ NFMs, b underwater oleophobicity of PAN and PAN@SiO₂ NFMs.

obviously with the increase in SiO₂ content. The increase in SiO₂ content enhanced the hydrophilicity and underwater oleophobicity of the PAN@SiO₂ NFMs, resulting in the increment of water flux in the process of oil-in-water emulsion separation. This is because amorphous SiO₂ sheets increase the content of hydrophilic groups, such as Si–OH, on the surface of the NFMs, leading to an increase in the hydrophilicity of the material.

Oil/water separation performance of the PAN@SiO₂ NFM

The experimental setup for oil-in-water emulsion separation is shown in Fig. 6a. A homemade automatic liquid filling device was used to maintain the vertical distance between the level of emulsion and the membrane was 10 cm, which ensured that the driving force generated by the gravity of the emulsion was constant (1 kPa) during the separation process. According to optical microscope images and droplet size distribution of toluene emulsion (Figs. S9 and S10), the droplet size of toluene emulsion is less

than 10 μm. To clearly illustrate the separation process, the oil phase was colored by Sudan III, and a typical separation process was recorded by video as shown in Video S3.

Toluene emulsion was prepared as model oil-in-water emulsion for the test of the separation performance of PAN and PAN@SiO₂ NFMs. The optical microscopy and digital photographic images of toluene SFE and SSE are shown in Fig. 6b. Before separation, numerous visible toluene droplets can be seen in the optical microscope images. Both milky white toluene SFE and SSE (uncolored) turned into transparent and no oil droplets were observed in the optical microscope images after separating by a PAN@SiO₂ NFM, demonstrating the effectiveness of the material for toluene emulsion separation.

The filtrates of toluene emulsions filtered by the PAN and PAN@SiO₂ NFMs were collected, and the residual TOC concentration was measured to calculate the separation efficiency (Fig. 7a). Both the PAN and PAN@SiO₂ NFMs showed excellent separation performance with low residual TOC concentration (less than 40 mg L⁻¹) and high separation efficiency (> 99.50%). Compared with the PAN NFM, the fluxes of PAN@SiO₂ NFMs increased significantly due to the hydrophilicity of SiO₂. With increasing SiO₂ content, the fluxes of PAN@SiO₂ NFMs increased first because of the hydrophilicity of SiO₂ and then decreased because the pore was blocked by the excess SiO₂. Among them, P@S-3 reached the highest value of 3994.3 ± 356.0 L m⁻² h⁻¹, which is 8.5 times higher than that of the pure PAN NFM (470 ± 29.5 L m⁻² h⁻¹). This result indicated that PAN@SiO₂ NFMs could be an efficient membrane for toluene emulsion separation.

The surfactant contains water-soluble polar groups and oil-soluble aliphatic chains, which are located at the oil/water interface and can significantly reduce the surface energy. The amphiphilic surfactants could be adsorbed by the membrane, making oil droplet removal challenging [17]. For the performance of PAN and PAN@SiO₂ NFMs for toluene SSE separation, the results are shown in Fig. 7b. Compared with the separation of toluene SFE, the fluxes of all NFMs for SSE emulsion separation decreased by a large margin and the residual TOC concentration of the filtrate increased. The fluxes of PAN@SiO₂ NFMs for SSE emulsion separation were still higher than that of PAN NFM, and the separation efficiency was also higher than 99.5%. The flux and separation efficiency

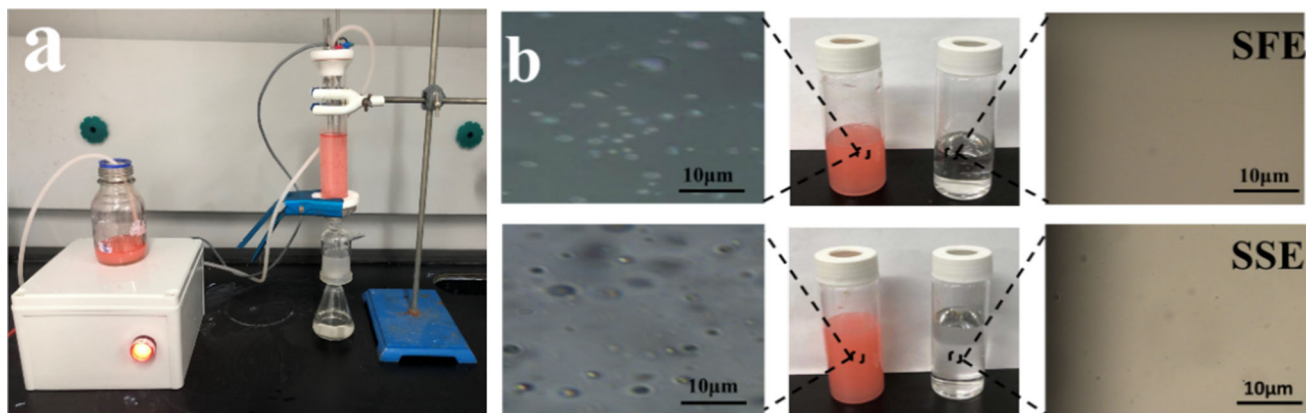


Figure 6 **a** Photograph of the experimental setup for oil-in-water emulsion separation, **b** optical microscope and digital photographic images of the toluene SFE and SSE (colored) before and after separation by a PAN@SiO₂ NFM.

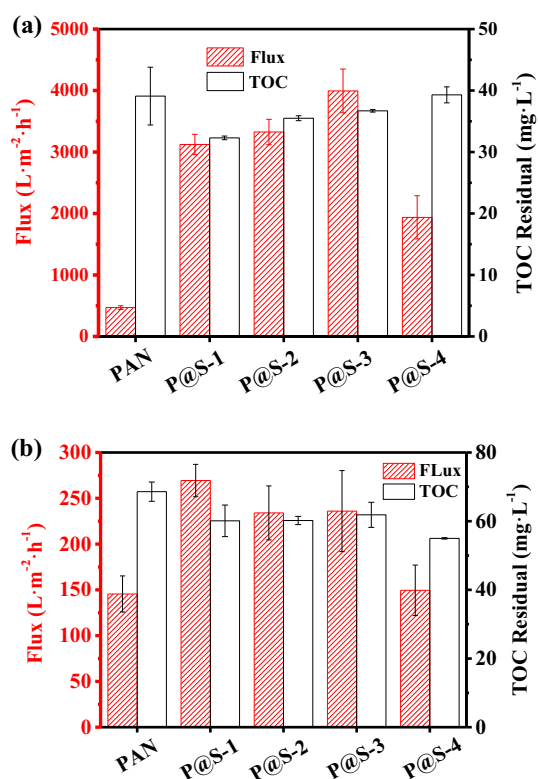


Figure 7 Flux and residual TOC concentration of filtrate from: **a** toluene SFE and **b** toluene SSE separated by PAN and PAN@SiO₂ NFMs.

of PAN@SiO₂ NFM for toluene SSE were compared with other membranes reported in the literature (Table 2). The PAN@SiO₂ NFM demonstrated a relatively high flux at a low driving force (1 kPa) compared with other emulsion separation membranes, indicating the PAN@SiO₂ NFM is a promising material for oil-in-water emulsion separation.

For an emulsion separation membrane, handling a wide variety of emulsions is necessary to make it universally available. Thus, the performance of the PAN@SiO₂ NFM for other emulsion separation was tested. *N*-heptane, paraffin liquid, *n*-hexane and xylene oil-in-water SFEs and SSEs were prepared, of which the ratio of oil to water was same as the toluene SFE and SSE. In the previous experiments, it was found that the P@S-3 NFM was the best material that had the highest flux. Thus, P@S-3 NFM was chosen as the tested NFM. The residual TOC concentrations of the filtrates from other four SFEs were all below 35 mg L⁻¹ (Fig. 8a), and all the separation efficiency exceeded 99.68%, indicating the excellent performance of P@S-3 NFM for emulsion separation. Except for *n*-heptane and paraffin liquid SFEs, the flux of P@S-3 NFM for the other three SFE separation were all higher than 2500 L m⁻² h⁻¹, suggesting the as-prepared PAN@SiO₂ NFMs could be suitable for rapid emulsion separation. Compared with the SFE separation, due to the effect of the surfactant, the fluxes of P@S-3 NFM also decreased by a large margin for the different SSE separation and the residual TOC concentration of the filtrate increased (Fig. 8b), but the separation efficiency was still high than 99%. Therefore, it is expected that the PAN@SiO₂ NFMs are suitable for the separation of a variety of oil-in-water emulsions.

Cyclic stability of the PAN@SiO₂ NFM for oil/water separation

Considering the inevitable membrane fouling, the flux and separation efficiency of membrane would

Table 2 Performance of PAN@SiO₂ NFM and other materials reported in the literature for SSE separation

Materials	Flux (L m ⁻² h ⁻¹ kPa ⁻¹)	Separation efficiency	Reference
M-PVDF membrane	200	99.9%	[17]
PVDF _{T-water} membrane	26	98.5%	[41]
TCNC membrane	17	99.9%	[42]
CA + SeP/GO membrane	19.1	98%	[43]
PAN/HPEI/PDA ENF	17.8	98.5%	[44]
GO/SiO ₂ membrane	45.5	99%	[34]
Nylon 6/SiO ₂ composite membrane	48.14	99%	[35]
PAN@SiO ₂ NFM	269.4	99.5%	This work

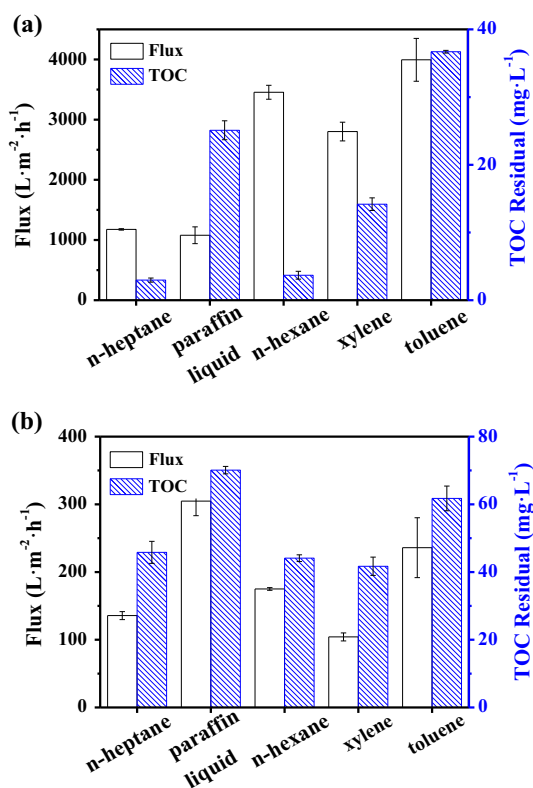


Figure 8 Flux and residual TOC concentration of the filtrate from different kinds of **a** SFEs and **b** SSEs separated by P@S-3 NFM.

gradually decline, limiting the membrane separation performance. Therefore, cyclic stability is another important factor to evaluate the membrane separation performance. To test the performance stability of the prepared NFMs for oil-in-water separation, the flux and residual TOC concentration were measured for ten successive cycles of toluene emulsion separation (Fig. 9). It was found that after ten cycles the decrease in flux and the increment in residual TOC concentration were insignificant because the hydrophilic surface could relieve the membrane fouling. The membrane fluxes were kept stable at

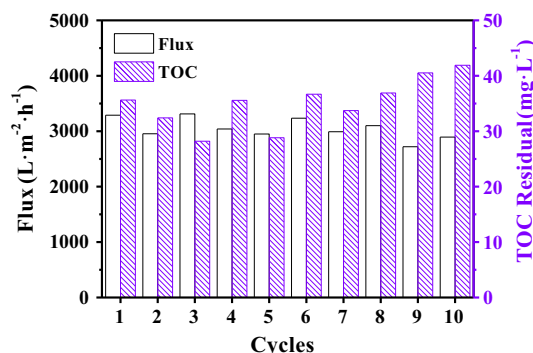


Figure 9 Flux of PAN@SiO₂ NFM for toluene emulsion separation and residual TOC concentration of the filtrate in ten successive cycles testing.

approximately 3000 L m⁻² h⁻¹, and the residual TOC concentration of the filtrate remained stable at about 30 mg L⁻¹ in ten cycles. These results demonstrated that the PAN@SiO₂ NFM has great stability for continuous oil-in-water emulsion separation, indicating this composite material could be an excellent emulsion separation membrane.

Conclusions

Large flux and high separation efficiency are two key parameters for excellent emulsion separation membranes. A highly efficient emulsion separation membrane was prepared via a facile sol-gel strategy to composite amorphous SiO₂ sheets on a PAN NFM surface. The as-prepared PAN@SiO₂ NFMs were highly efficient for emulsion separation. For toluene oil-in-water emulsion separation, a high flux of 3994.3 ± 356.0 L m⁻² h⁻¹ and separation efficiency (99.50%) were achieved under a very low gravity-driven pressure of 1 kPa. The changes in flux and separation efficiency in ten successive cycle tests were insignificant. For other oil-in-water emulsion

separation, such as *n*-heptane, paraffin liquid, *n*-hexane and xylene, all the separation efficiency exceeded 99.68%, indicating that the PAN@SiO₂ NFM can be a promising material for the efficient separation of various kinds of oil-in-water emulsions.

Acknowledgements

The authors acknowledge the financial support from the National Natural Science Foundation of China (Grant Nos. 51578525, 51978639 and 153000136), the FJIRSM&IUE Joint Research Fund (Grant No RHZX-2018-003), the Science and Technology Planning Project of Xiamen City (Grant No. 3502Z20193074) and the STS Project of Science and Technology Program of Fujian Province (Grant No. 2018T3002).

Compliance with ethical standards

Conflict of interest The authors declare no competing financial interest.

Electronic supplementary material: The online version of this article (<https://doi.org/10.1007/s10853-020-05155-8>) contains supplementary material, which is available to authorized users.

References

- [1] Shannon MA, Bohn PW, Elimelech M, Georgiadis JG, Marinas BJ, Mayes AM (2008) Science and technology for water purification in the coming decades. *Nature* 452(7185):301–310. <https://doi.org/10.1038/nature06599>
- [2] Padaki M, Surya MR, Abdullah MS, Misdan N, Moslehyani A, Kassim MA, Hilal N, Ismail AF (2015) Membrane technology enhancement in oil–water separation. A review *Desalination* 357:197–207. <https://doi.org/10.1016/j.desal.2014.11.023>
- [3] Zhang J, Xue Q, Pan X, Jin Y, Lu W, Ding D, Guo Q (2017) Graphene oxide/polyacrylonitrile fiber hierarchical-structured membrane for ultra-fast microfiltration of oil-water emulsion. *Chem Eng J* 307:643–649. <https://doi.org/10.1016/j.cej.2016.08.124>
- [4] Zhang C, He S, Wang D, Xu F, Zhang F, Zhang G (2018) Facile fabricate a bioinspired Janus membrane with heterogeneous wettability for unidirectional water transfer and controllable oil–water separation. *J Mater Sci* 53(20):14398–14411. <https://doi.org/10.1007/s10853-018-2659-8>
- [5] Fan JB, Song Y, Wang S, Meng J, Yang G, Guo X, Feng L, Jiang L (2015) Directly coating hydrogel on filter paper for effective oil-water separation in highly acidic, alkaline, and salty environment. *Adv Funct Mater* 25(33):5368–5375. <https://doi.org/10.1002/adfm.201501066>
- [6] Zhang L, Ying H, Yan S, Zhan N, Guo Y, Fang W (2018) Hyperbranched poly(amido amine) demulsifiers with ethylenediamine/1,3-propanediamine as an initiator for oil-in-water emulsions with microdroplets. *Fuel* 226:381–388. <https://doi.org/10.1016/j.fuel.2018.03.196>
- [7] Etchepare R, Oliveira H, Azevedo A, Rubio J (2017) Separation of emulsified crude oil in saline water by dissolved air flotation with micro and nanobubbles. *Sep Purif Technol* 186:326–332. <https://doi.org/10.1016/j.seppur.2017.06.007>
- [8] Li Y, Feng Z, He Y, Fan Y, Ma J, Yin X (2018) Facile way in fabricating a cotton fabric membrane for switchable oil/water separation and water purification. *Appl Surf Sci* 441:500–507. <https://doi.org/10.1016/j.apsusc.2018.02.060>
- [9] Yeber M, Paul E, Soto C (2012) Chemical and biological treatments to clean oily wastewater: optimization of the photocatalytic process using experimental design. *Desalin Water Treat* 47(1–3):295–299. <https://doi.org/10.1080/19443994.2012.696413>
- [10] He J, Zhang Y, Wang J, Ma L, Zhao Y, Zhou Y, Yang Z, Qu M (2020) Eco-friendly, magnetic-driven, superhydrophobic sponge for oil/water separation and emulsion purification. *J Mater Sci* 55(15):6708–6720. <https://doi.org/10.1007/s10853-020-04462-4>
- [11] Zhu X, Dudchenko A, Gu X, Jassby D (2017) Surfactant-stabilized oil separation from water using ultrafiltration and nanofiltration. *J Membr Sci* 529:159–169. <https://doi.org/10.1016/j.memsci.2017.02.004>
- [12] Abadi SRH, Sebzari MR, Hemati M, Rekabdar F, Mohammedi T (2011) Ceramic membrane performance in micro-filtration of oily wastewater. *Desalination* 265(1–3):222–228. <https://doi.org/10.1016/j.desal.2010.07.055>
- [13] Gao S, Zhu Y, Wang J, Zhang F, Li J, Jin J (2018) Layer-by-layer construction of Cu²⁺/Alginate multilayer modified ultrafiltration membrane with bioinspired superwetting property for high-efficient crude-oil-in-water emulsion separation. *Adv Funct Mater* 28(49):1801944. <https://doi.org/10.1002/adfm.201801944>
- [14] Liu X, Ong SL, Ng HY (2016) Fabrication of mesh-embedded double-skinned substrate membrane and enhancement of its surface hydrophilicity to improve anti-fouling performance of resultant thin-film composite forward osmosis membrane. *J Membr Sci* 511:40–53. <https://doi.org/10.1016/j.memsci.2016.03.015>

- [15] Wang Q, Cui J, Liu S, Gao J, Lang J, Li C, Yan Y (2019) Facile preparation of halloysite nanotube-modified polyvinylidene fluoride composite membranes for highly efficient oil/water emulsion separation. *J Mater Sci* 54(11):8332–8345. <https://doi.org/10.1007/s10853-019-03482-z>
- [16] Ge J, Zhang J, Wang F, Li Z, Yu J, Ding B (2017) Super-hydrophilic and underwater superoleophobic nanofibrous membrane with hierarchical structured skin for effective oil-in-water emulsion separation. *J Mater Chem A* 5(2):497–502. <https://doi.org/10.1039/c6ta07652a>
- [17] Liao Y, Tian M, Wang R (2017) A high-performance and robust membrane with switchable super-wettability for oil/water separation under ultralow pressure. *J Membr Sci* 543:123–132. <https://doi.org/10.1016/j.memsci.2017.08.056>
- [18] Huang ZM, Zhang YZ, Kotaki M, Ramakrishna S (2003) A review on polymer nanofibers by electrospinning and their applications in nanocomposites. *Compos Sci Technol* 63(15):2223–2253. [https://doi.org/10.1016/s0266-3538\(03\)00178-7](https://doi.org/10.1016/s0266-3538(03)00178-7)
- [19] Greiner A, Wendorff JH (2007) Electrospinning: a fascinating method for the preparation of ultrathin fibers. *Angew Chem Int Ed Engl* 46(30):5670–5703. <https://doi.org/10.1002/anie.200604646>
- [20] Ondarcuhu T, Joachim C (1998) Drawing a single nanofibre over hundreds of microns. *Europhys Lett* 42(2):215–220. <https://doi.org/10.1209/epl/i1998-00233-9>
- [21] Liu G, Ding J, Qiao L, Guo A, Dymov BP, Gleeson JT, Hashimoto T, Saijo K (1999) Polystyrene-block-poly(2-cin-namoyl ethyl methacrylate) nanofibers—preparation, characterization, and liquid crystalline properties. *Chem Eur J* 5(9):2740–2749. [https://doi.org/10.1002/\(sici\)1521-3765\(19990903\)5:9<2740:aid-chem2740>3.0.co;2-v](https://doi.org/10.1002/(sici)1521-3765(19990903)5:9<2740:aid-chem2740>3.0.co;2-v)
- [22] Peter X, Ma RZ (1998) Synthetic nano-scale fibrous extracellular matrix. *J Biomed Mater Res* 46(1):60–72. [https://doi.org/10.1002/\(sici\)1097-4636\(199907\)46:1<60:aid-jbm7>3.0.co;2-h](https://doi.org/10.1002/(sici)1097-4636(199907)46:1<60:aid-jbm7>3.0.co;2-h)
- [23] Kaviyarasu K, Manikandan E, Nuru ZY, Maaza M (2015) Investigation on the structural properties of CeO₂ nanofibers via CTAB surfactant. *Mater Lett* 160:61–63. <https://doi.org/10.1016/j.matlet.2015.07.099>
- [24] Kaviyarasu K, Manikandan E, Nuru ZY, Maaza M (2015) Quantum confinement of lead titanate nanocrystals by wet chemical method. *J Alloy Compd* 649:50–53. <https://doi.org/10.1016/j.jallcom.2015.07.099>
- [25] Lokesh K, Kavitha G, Manikandan E, Mani GK, Kaviyarasu K, Rayappan JBB, Ladhumananandasivam R, Sundeepp Aanand J et al (2016) Effective ammonia detection using n-ZnO/p-NiO heterostructured nanofibers. *IEEE Sens J* 16(8):2477–2483. <https://doi.org/10.1109/jnsen.2016.2517085>
- [26] Sathiyamoorthy S, Girijakumari G, Kannan P, Venugopal K, Shanmugam ST, Veluswamy P, Wael KD, Ikeda H (2018) Tailoring the functional properties of polyurethane foam with dispersions of carbon nanofiber for power generator applications. *Appl Surf Sci* 449:507–513. <https://doi.org/10.1016/j.apsusc.2018.01.088>
- [27] Veluswamy P, Sathiyamoorthy S, Khan F, Ghosh A, Abhijit M, Hayakawa Y, Ikeda H (2017) Incorporation of ZnO and their composite nanostructured material into a cotton fabric platform for wearable device applications. *Carbohydr Polym* 157:1801–1808. <https://doi.org/10.1016/j.carbpol.2016.11.065>
- [28] Wu J, Wang N, Zhao Y, Jiang L (2013) Electrospinning of multilevel structured functional micro-/nanofibers and their applications. *J Mater Chem A* 1 (25). <https://doi.org/10.1039/c3ta10451f>
- [29] Frenot A, Chronakis IS (2003) Polymer nanofibers assembled by electrospinning. *Curr Opin Colloid In* 8(1):64–75. [https://doi.org/10.1016/s1359-0294\(03\)00004-9](https://doi.org/10.1016/s1359-0294(03)00004-9)
- [30] Li K, Hou D, Fu C, Wang K, Wang J (2019) Fabrication of PVDF nanofibrous hydrophobic composite membranes reinforced with fabric substrates via electrospinning for membrane distillation desalination. *J Environ Sci (China)* 75:277–288. <https://doi.org/10.1016/j.jes.2018.04.002>
- [31] Chen T, Duan M, Fang S (2016) Fabrication of novel superhydrophilic and underwater superoleophobic hierarchically structured ceramic membrane and its separation performance of oily wastewater. *Ceram Int* 42(7):8604–8612. <https://doi.org/10.1016/j.ceramint.2016.02.090>
- [32] Gong Z, Yang N, Chen Z, Jiang B, Sun Y, Yang X, Zhang L (2020) Fabrication of meshes with inverse wettability based on the TiO₂ nanowires for continuous oil/water separation. *Chem Eng J* 380. <https://doi.org/10.1016/j.cej.2019.122524>
- [33] Qin A, Li X, Zhao X, Liu D, He C (2015) Engineering a highly hydrophilic PVDF membrane via binding TiO₂ nanoparticles and a PVA layer onto a membrane surface. *ACS Appl Mater Inter* 7(16):8427–8436. <https://doi.org/10.1021/acsami.5b00978>
- [34] Sun J, Bi H, Su S, Jia H, Xie X, Sun L (2018) One-step preparation of GO/SiO₂ membrane for highly efficient separation of oil-in-water emulsion. *J Membr Sci* 553:131–138. <https://doi.org/10.1016/j.memsci.2018.02.029>
- [35] Islam MS, McCutcheon JR, Rahaman MS (2017) A high flux polyvinyl acetate-coated electrospun nylon 6/SiO₂ composite microfiltration membrane for the separation of oil-in-water emulsion with improved antifouling performance.

- J Membr Sci 537:297–309. <https://doi.org/10.1016/j.memsci.2017.05.019>
- [36] Ngang HP, Ahmad AL, Low SC, Ooi BS (2017) Preparation of thermoresponsive PVDF/SiO₂-PNIPAM mixed matrix membrane for saline oil emulsion separation and its cleaning efficiency. *Desalination* 408:1–12. <https://doi.org/10.1016/j.desal.2017.01.005>
- [37] Yang S, Si Y, Fu Q, Hong F, Yu J, Al-Deyab SS, El-Newehy M, Ding B (2014) Superwetting hierarchical porous silica nanofibrous membranes for oil/water microemulsion separation. *Nanoscale* 6(21):12445–12449. <https://doi.org/10.1039/c4nr04668d>
- [38] Tai MH, Gao P, Tan BY, Sun DD, Leckie JO (2014) Highly efficient and flexible electrospun carbon-silica nanofibrous membrane for ultrafast gravity-driven oil-water separation. *ACS Appl Mater Inter* 6(12):9393–9401. <https://doi.org/10.1021/am501758c>
- [39] Naseeb N, Mohammed AA, Laoui T, Khan Z (2019) A novel PAN-GO-SiO₂ hybrid membrane for separating oil and water from emulsified mixture. *Materials (Basel)* 12(2). <https://doi.org/10.3390/ma12020212>
- [40] Karki HP, Kafle L, Ojha DP, Song JH, Kim HJ (2019) Cellulose/polyacrylonitrile electrospun composite fiber for effective separation of the surfactant-free oil-in-water mixture under a versatile condition. *Sep Purif Technol* 210:913–919. <https://doi.org/10.1016/j.seppur.2018.08.053>
- [41] Zuo JH, Cheng P, Chen XF, Yan X, Guo YJ, Lang WZ (2018) Ultrahigh flux of polydopamine-coated PVDF membranes quenched in air via thermally induced phase separation for oil/water emulsion separation. *Sep Purif Technol* 192:348–359. <https://doi.org/10.1016/j.seppur.2017.10.027>
- [42] Cheng Q, Ye D, Chang C, Zhang L (2017) Facile fabrication of superhydrophilic membranes consisted of fibrous tunicate cellulose nanocrystals for highly efficient oil/water separation. *J Membr Sci* 525:1–8. <https://doi.org/10.1016/j.memsci.2016.11.084>
- [43] Li F, Gao R, Wu T, Li Y (2017) Role of layered materials in emulsified oil/water separation and anti-fouling performance of modified cellulose acetate membranes with hierarchical structure. *J Membr Sci* 543:163–171. <https://doi.org/10.1016/j.memsci.2017.08.053>
- [44] Wang J, La H, Yan K, Zhang L, Yu QJ (2018) Polydopamine nanocluster decorated electrospun nanofibrous membrane for separation of oil/water emulsions. *J Membr Sci* 547:156–162. <https://doi.org/10.1016/j.memsci.2017.10.028>

Publisher's Note Springer Nature remains neutral with regard to jurisdictional claims in published maps and institutional affiliations.